Molecular Biology of the Cell
Vol. 12, 2519–2533, August 2001

Cnm67p Is a Spacer Protein of the *Saccharomyces cerevisiae* Spindle Pole Body Outer Plaque

Florian Schaerer,* Garry Morgan,† Mark Winey,† and Peter Philippsen*‡

*Molecular Microbiology, Biozentrum der Universität, CH-4056 Basel, Switzerland; and
†MCD Biology, University of Colorado, Boulder, Colorado 80309

Submitted February 26, 2001; Revised May 1, 2001; Accepted May 15, 2001
Monitoring Editor: Tim Stearns

In *Saccharomyces cerevisiae*, the spindle pole body (SPB) is the functional homolog of the mammalian centrosome, responsible for the organization of the tubulin cytoskeleton. Cytoplasmic (astral) microtubules essential for the proper segregation of the nucleus into the daughter cell are attached at the outer plaque on the SPB cytoplasmic face. Previously, it has been shown that Cnm67p is an integral component of this structure; cells deleted for *CNM67* are lacking the SPB outer plaque and thus experience severe nuclear migration defects. With the use of partial deletion mutants of *CNM67*, we show that the N- and C-terminal domains of the protein are important for nuclear migration. The C terminus, not the N terminus, is essential for Cnm67p localization to the SPB. On the other hand, only the N terminus is subject to protein phosphorylation of a yet unknown function. Electron microscopy of SPB serial thin sections reveals that deletion of the N- or C-terminal domains disturbs outer plaque formation, whereas mutations in the central coiled-coil domain of Cnm67p change the distance between the SPB core and the outer plaque. We conclude that Cnm67p is the protein that connects the outer plaque to the central plaque embedded in the nuclear envelope, adjusting the space between them by the length of its coiled-coil.

INTRODUCTION

Precise positioning of the nucleus and alignment of the spindle are important prerequisites for the correct partitioning of the genetic material between mother and daughter cell during mitosis in the yeast *Saccharomyces cerevisiae*. These processes depend on astral microtubules (Huffaker *et al.*, 1988; Palmer *et al.*, 1992; Sullivan and Huffaker, 1992; Carminati and Stearns, 1997; Shaw *et al.*, 1997), on microtubule motors (Eshel *et al.*, 1993; Li *et al.*, 1993; Carminati and Stearns, 1997; Cottingham and Hoyt, 1997; DeZwaan *et al.*, 1997), and on cortical determinants (Farkasovsky and Küntzel, 1995; Miller and Rose, 1998; Miller *et al.*, 1999; reviewed by Schaerer-Brodbeck and Riezman, 2000). Microtubule organizing centers (MTOCs) play an important role in this process because they are responsible for the nucleation and anchoring of microtubules into a bipolar array and thus for positioning of the nucleus within the cell during cell division and differentiation (reviewed by Kellogg *et al.*, 1994; Pereira and Schiebel, 1997; Palazzo and Schatten, 2000). Despite being a morphologically diverse group of organelles, MTOC functions are largely conserved. In the yeast *S. cerevisiae*, the role of the MTOC is served by the spindle pole body (SPB), a multilaminar structure permanently embedded in the nuclear envelope (Winey and Byers, 1993; Kilmartin, 1994; Snyder, 1994; reviewed by Francis and Davis, 2000). Spindle, or nuclear, microtubules emanate from the nuclear side of the SPB, and astral, or cytoplasmic, microtubules are organized by its cytoplasmic face. In the G1 phase of the cell cycle these are also attached at the half-bridge, an appendage on the side of the SPB that is a modification of the nuclear membrane. After SPB duplication and separation, cytoplasmic microtubules are organized by the outer plaque of the SPB (Byers and Goetsch, 1975; Byers, 1981; Kilmartin, 1994; Snyder, 1994).

With a combination of experimental approaches, components have been identified and mapped to the three main electron-dense layers of the SPB, which initially had been characterized by electron microscopy (Moens and Rapport, 1971; Byers and Goetsch, 1975). Matrix-assisted laser desorption/ionization finally allowed the identification and subsequent localization of additional SPB core and associated proteins in a large-scale approach (Wigge *et al.*, 1998). The central crystalline plaque is composed of the *SPC42* gene product (Donaldson and Kilmartin, 1996; Bullitt *et al.*, 1997) and is the layer that anchors the SPB in the nuclear membrane. The inner (nuclear) plaque component Spc110p (Rout and Kilmartin, 1990) has a spacer function (Kilmartin *et al.*, 1993) and bears the attachment sites for the γ-tubulin complexes and thus for the nuclear microtubules (Knop and Schiebel, 1997; Sundberg and Davis, 1997). Components required for the formation of the outer (cytoplasmic) plaque and anchoring of microtubules to this structure include Cnm67p (Brachat *et al.*, 1998), Nud1p (Adams and Kilmartin,

‡ Corresponding author. E-mail address: Peter.Philippsen@unibas.ch.

© 2001 by The American Society for Cell Biology

Table 1. Strains used in this study

Strain	Relevant genotype	Source or reference
FY1679	*MATa/α his3Δ200/HIS3 leu2Δ1/LEU2 trp1Δ63/TRP1 ura3-52/ura3-52*	B. Dujon
CEN.PK2	*MATa/α his3Δ1/his3Δ1 leu2-3,112/leu2-3,112 trp1-289/trp1-289 ura3-52/ura3-52*	K.D. Entian
ABY132	*MATa/α CNM67::3HA-kanMX6/CNM67::3HA-kanMX6 his3Δ1/his3Δ1 leu2-3,112/leu2-3,112 trp1-289/trp1-289 ura3-52/ura3-52*	Brachat *et al*., 1998
FSY020	*MATa/α cnm67::kanMX4/cnm67::HIS3MX6 HHF2::GFP-kanMX6/HHF2 ura3-52/ura3-52 his3Δ200/his3Δ200 LEU2/leu2Δ1 trp1Δ63/trp1Δ63*	This study
FSY023	*MATa/α HHF2::GFP-kanMX6/HHF2 ura3-52/ura3-52 his3Δ200/his3Δ200 LEU2/leu2Δ1 trp1Δ63/trp1Δ63*	This study
FSY034	*MATa/α cnm67::kanMX4/cnm67::HIS3MX6 ura3-52/ura3-52 leu2Δ1/leu2Δ1 his3Δ200/his3Δ200 trp1Δ63/trp1Δ1*	This study
FSY126 #A1	*MATa cnm67::klTRP1 his3Δ1 leu2-3,112 trp1-289 ura3-52*	This study
FSY170	*MATa cnm67::pFS092 his3Δ1 leu2-3,112 trp1-289 ura3-52*	This study
FSY174	*MATa cnm67::pFS118 his3Δ1 leu2-3,112 trp1-289 ura3-52*	This study
FSY175	*MATa cnm67::pFS119 his3Δ1 leu2-3,112 trp1-289 ura3-52*	This study
FSY182	*MATa cnm67::pFS131 his3Δ1 leu2-3,112 trp1-289 ura3-52*	This study
FSY184	*MATa cnm67::pFS133 his3Δ1 leu2-3,112 trp1-289 ura3-52*	This study

1999; Gruneberg *et al*., 2000), and Spc72, which, similar to Spc110p of the inner plaque, has a γ-tubulin complex binding domain (Chen *et al*., 1998; Knop and Schiebel, 1998; Souès and Adams, 1998).

In contrast to the SPB components Nud1p and Spc72p, which can be found associated to both half bridge and outer plaque structures, Cnm67p was localized exclusively to the cytoplasmic side of the SPB itself (Wigge *et al*., 1998; Adams and Kilmartin, 1999). Cnm67p was found to be important for the integrity of this substructure; cells deleted for *CNM67* are devoid of the SPB outer plaque and therefore lack the attachment sites for cytoplasmic microtubules. Consequently, these cells experience a severe nuclear migration defect, and their survival arises from a rescue pathway provided by cytoplasmic microtubules emanating from the half bridge (Brachat *et al*., 1998). The role of Cnm67p on the outer plaque of the SPB, however, is still unclear.

In this study, we functionally dissect the multidomain protein Cnm67p. The nuclear migration function, the localization determinants, and the domains essential for its phosphorylation have been mapped. We also present several lines of evidence that Cnm67p is the linker element between the central and outer plaques of the SPB and that Cnm67p sets the space between these two substructures.

MATERIALS AND METHODS

Yeast Strains and Media

Yeast strains used in this study are listed in Table 1. Unless mentioned otherwise, strains without plasmids were grown in complete medium YPD (2% yeast extract, 1% peptone, 2% glucose, 2% agar for solid media). Strains carrying plasmids were grown in SD dropout medium (6.7 g/l yeast nitrogen base; Difco, Detroit, MI), 0.6 g/l complete supplement mixture minus histidine, leucine, tryptophane, uracil [Bio101, Vista, CA], 2% glucose), supplemented with amino acids and agar as required. Yeast cells were transformed with the use of a lithium acetate/polyethylene glycol protocol (Schiestl and Gietz, 1989).

For one-step gene deletions and taggings, a polymerase chain reaction (PCR)-based method was used to generate cassettes with short targeting homologies (Wach *et al*., 1994). *CNM67* was deleted with a cassette synthesized with the use of the templates pFA6a-*kanMX4* (Wach *et al*., 1994), pFA6a-*HIS3MX6* (Wach *et al*., 1997), or pYM3 (Knop *et al*., 1999) with the primer sets ΔF and ΔR (*cnm67::kanMX6* and *cnm67::HIS3MX6*) or ΔF(TRP1) and ΔR (*cnm67::klTRP1* deletion), respectively. Genomic tagging of *CNM67* with green fluorescent protein (GFP) or 3HA was done with the primers NL225c-c-fus5′ and NL225c-c-fus3′ in conjunction with the template plasmids pFA6a-*GFP(S65T)-kanMX6* (Wach *et al*., 1997) and pFA6a-*3HA-kanMX6* (Brachat *et al*., 1998). For the genomic Histone H4-GFP fusions, the template pFA6a-*GFP(S65T)-kanMX6* and the primers H4-c-fus5′ and H4-c-fus3′ were used. Correct integration was verified by analytical PCR (Huxley *et al*., 1990; Wach *et al*., 1994).

The yeast strain FSY126 #A1 resulted from sporulation of a *cnm67::klTRP1* deletion in the CEN.PK2 background. To construct the strains FSY170, FSY174, FSY175, FSY182, FSY184, and FSY188 carrying a copy of the mutated *cnm67* alleles genomically integrated at the original *CNM67* locus, *cnm67* integration cassettes with long regions of homology were excised from pFS092, pFS118, pFS119, pFS131, and pFS133, respectively, purified, and transformed into FSY126 #A1. Strains with replacement of the genomic *cnm67::klTRP1* allele where identified by screening for $HIS3^+$ $trp1^-$ transformants. This strategy allowed to positively select for the integration via *HIS3* and to verify for a complete integration of the mutated open reading frame by the replacement of the *klTRP1* marker. Expression of the mutant alleles was tested by Western blot analysis (described below).

DNA Techniques and Plasmid Constructions

All DNA manipulations were performed according to standard techniques (Sambrook *et al*., 1989) unless otherwise specified. Restriction enzymes, Klenow, T4 DNA polymerase, calf intestinal phosphatase (CIP), T4 polynucleotide kinase (PNK), mung bean nuclease, and T4 DNA ligase were obtained from New England Biolabs, Beverly, MA. All DNA fragments were purified with the QIAEX II or QIAQUICK gel purification kit (Qiagen, Chatsworth, CA). Plasmids were purified with the alkaline lysis protocol (Sambrook *et al*., 1989), and transformation of *Escherichia coli* for plasmid propagation was performed by electroporation (Dower *et al*., 1988). All PCRs for cloning purposes were performed with Vent DNA polymerase with proofreading activity (New England Biolabs) and double-strand sequenced. Primers used for PCR are listed in Table 2.

Table 2. Oligonucleotides used in this study

Primer	Sequence
ΔF	5′-GGC ACT AGT ATG CTT GAT CCG TAA ATT TCT TTA GAT TCA TTC *ATC GAT GAA TTC GAG CTC*-3′
ΔR	5′-GCG CAG CTG ATT TCG ATT TAA TGA ATT TTC CAT TTC ATG AGC *CGT ACG CTG CAG GTC GAC*-3′
ΔF(klTRP1)	5′-GGC ACT AGT ATG CTT GAT CCG TAA ATT TCT TTA GAT TCA TTG *CTT CGT ACG CTG CAG GTC G*-3′
NL225c-c-fus5′	5′-CTG GAC CAT CTG TAT GAT CAT ATC CTG GAG AAG ATG GTG AAG *GGT CGA CGG ATC CCC GGG*-3′
NL225c-c-fus3′	5′-TAT ACA TAC TTC CTA GAA TAT AAT TTA ATC TTA TAC CTT AAC *ATC GAT GAA TTC GAG CTC G*-3′
H4-c-fus5′	5′-GCT TTG AAG AGA CAA GGT AGA ACC TTA TAT GGT TTC *GGT GGT GGT CGA CGG ATC CCC GGG*-3′
H4-c-fus3′	5′-CAT ACA TAA GGT TCT ATT ATA TTC CCA ATA GAA TGA TCG TTA *CAT CGA TGA ATT CGA GCT CG*-3′
GA7_F1	5′-ggg GCC GGT GCA GGC GCT GGA GCT GGC GCC GGT GCT GGC GCA-3′
GA7_R1	5′-TGC GCC AGC ACC GGC GCC AGC TCC AGC GCC TGC ACC GGC ccc-3′
3GA_3HA_F1	5′-ggg GCT GGT GCC GGT GCA *TAC CCA TAC GAT GTT CCT GAC*-3′
3GA_YGFP_F1	5′-ggg GCT GGT GCC GGT GCA *TCT AAA GGT GAA GAA TTA TTC*-3′
6H_3HA_R2	5′-AGG CCT gat atc ATG GTG ATG ATG GTG ATG *AGC AGC GTA ATC TGG AAC GTC*-3′
6H_YGFP_R2	5′-AGG CCT gat atc ATG GTG ATG ATG GTG ATG *TTT GTA CAA TTC ATC CAT ACC*-3′
MF2	5′-GGg gta ccC CAT TTT CCA AGC TTT TAA TCC-3′
MR2	5′-CGg gat ccC GAT ATT GTA GGG CCT TTT TAC-3′
SF1	5′-GAG AAG ATG ccc ggg TAA TTT TTA TTA ACG GAG-3′
SR1	5′-CTC CGT TAA TAA AAA TTA ccc ggg CAT CTT CTC-3′
DF1	5′-CGA AAG AGG ATT TTC GAa tgc atG TAT TGA TTG AAA ACC T-3′
DF2	5′-AAT ATC CTA ATA TTA AAG GGa gat ctC TTT CCA AAC AGA A-3′
DF3	5′-CAA TCG ATG AGA AGg aat tcA CTT CTG AAA GGA TTA CAA T-3′
S1_DF4	5′-TTG GAA ACT TAG AGc ccg ggT AAT TTT TAT TAA CGG AGT C-3′
DF5	5′-CAG GTC TTT TGT ACA cca tgg TAG AAA ATG TGA TAC TGG G-3′
DR1	5′-AGG TTT TCA ATC AAT ACa tgc atT CGA AAA TCC TCT TTC G-3′
DR2	5′-TTC TGT TTG GAA AGa gat ctC CCT TTA ATA TTA GGA TAT T-3′
DR3	5′-ATT GTA ATC CTT TCA GAA GTg aat tcC TTC TCA TCG ATT G-3′
S1_DR4	5′-GAC TCC GTT AAT AAA AAT TAc ccg ggC TCT AAG TTT CCA A-3′
DR5	5′-CCC AGT ATC ACA TTT TCT Acc atg gTG TAC AAA AGA CCT G-3′
5_R1	5′-ggg CAT TCG AAA ATC CTC TTT CG-3′
2coil_F	5′-G TAT CAA AAA AAA GTT ATT GAA TTG GG-3′
2coil_R	5′-A tgg cca ATT TCC CTC TAA GTT TCC AAA TCG-3′
DF5	5′-CAG GTC TTT TGT ACA cca tgg TAG AAA ATG TGA TAC TGG G-3′
DR1	5′-AGG TTT TCA ATC AAT ACa tgc atT CGA AAA TCC TCT TTC G-3′
MAF1	5′-CGG AGT CAA TAG ATA AAT TGT TGT AAT TGT AAC TAA AAA T*GC GCC ACT TCT AAA TAA GCG*-3′
MAR1	5′-ATG AAT ATT TTA TAC ATA CTT CCT AGA ATA TAA TTT AAT C*AT AGG CCA CTA GTG GAT CTG*-3′

Italic letters indicate homology to pFA6a plasmids; lower case letters indicate restriction sites introduced.

Plasmids used in this study are listed in Table 3. Tagging cassette plasmids were constructed by PCR of the inserts from pYGFP1 (yeast codon-enhanced GFP; Cormack *et al.*, 1997) template with primer pair 3GA_YGFP_F1/6H_YGFP_R2 for pFS040, and from pFA6a-3HA-kanMX6 template (Brachat *et al.*, 1998) with primers 3GA_3HA_F1/6H_3HA_R2 for pFS042, followed by phosphorylation of the ends of the PCR product with PNK, *Eco*RV cleavage of the 3′ end, and ligation into *Sma*I-*Eco*RV of pFA6a (Wach *et al.*, 1994). Annealed and PNK-phosphorylated oligonucleotides GA7_F1 and GA7_R1 were cloned into *Sma*I of pFS040 and pFS042, resulting in the nonrepetitive, nonpalindromic $(GA)_{10}$ linker derivatives pFS043 and pFS045.

The *CNM67* wild-type gene clone in pFS011 includes the open reading frame and 325-bp upstream and 385-bp downstream region that was amplified from cosmid14-6 with the use of the primers MF2 and MR2, both of which included restriction sites for *Kpn*I-*Bam*HI cloning into pRS414 (Sikorski and Hieter, 1989). A *Sma*I cloning site was introduced immediately 5′ of the termination codon of *CNM67* as follows. An upstream fragment with the use of MF2/Primer R (Primer R; see below) primer pair, and a downstream fragment with the use of Primer F/MR2 pair (Primer F; see below) were amplified separately. The primers were designed to yield PCR fragments having a homologous region of 40 bp, overlapping the codons to be mutated, that allowed annealing of the two PCR products. The products of this first PCR were mixed and used as template/primer in a second round of PCR with MF2/MR2 flanking primers, purified, and cloned *Kpn*I - *Bam*HI into pRS414. Primer F and Primer R were SF1 and SR1 with pFS011 as a template for the *Sma*I site insertion construct pFS019. Partial deletions of *CNM67* were constructed with the same technique with pFS019 as the template using the following primers F and R: DF1 and DR1 for Δcoil1 pFS025, DF2 and DR2 for Δcoil2 pFS026, DF3 and DR3 for Δcoil3 pFS027, DF4_S1 and DR4_S1 for ΔC pF028, and DF5 and DR5 for ΔN pFS029 deletions. *yEGFP1* and *3HA* tagging cassettes were released from pFS040, pFS042, or pFS045 with *Sma*I-*Eco*RV, purified, and cloned into the *Sma*I site of *CNM67* wild-type (wt) plasmid pFS019 or the partial deletions pFS025 to pFS029, yielding pFS022, pFS024, pFS048, and the 10 plasmids, pFS030 to pFS039, carrying either a *yEGFP* or *3HA* tagged version of the respective construct.

The C-terminal *CNM67* fragment in pFS049 was constructed with the use of pFS027 as the vector part, removing the fragment between the upstream polylinker and the coil3 deletion site by digesting pFS027 with *Eco*RI, a site that was included in the primers DF3 and DR3, followed by in-frame blunt-ending of the overhang with mung bean nuclease, and subsequent *Kpn*I cleavage. A phosphorylated and *Kpn*I-cleaved PCR-product of the primers MF2/DR5 representing the *CNM67* promoter and START codon region was then inserted in-frame. The tagged derivative pFS089 was constructed as described above.

Table 3. Plasmids used in this study

Plasmid	Markers/vector	Insert	Source or reference
pRS414	*Amp, ori, CEN, ARS, TRP1*		Sikorski and Hieter, 1989
pUC19	*Amp, ori*		Yanisch-Perron *et al*., 1985
pYGFP1	*Amp, ori*	*yEGFP1*(F64L, S65T)	Cormack *et al*., 1997
pFA6a-3HA-kanMX6	pFA6a	*3HA-TADH-kanMX6*	Brachat *et al*., 1998
pFA6a-GFP(S65T)-HIS3MX6	pFA6a	*GFP(S65T)-TADH-HIS3MX6*	Wach *et al*., 1997
pYM3	pFA6a	*6HA-klTRP1*	Knop *et al*., 1999
pFS040	pFA6a	$(GA)_3$-*yEGFP1-6H*	This study
pFS042	pFA6a	$(GA)_3$-*3HA-6H*	This study
pFS043	pFA6a	$(GA)_{10}$-*yEGFP1-6H*	This study
pFS045	pFA6a	$(GA)_{10}$-*3HA-6H*	This study
cosmid14-6	*Amp, ori*	19.054kb region of chromosome 14 left arm	Philippsen collection
pFS011	pRS414	*CNM67*	This study
pFS019	pRS414	*CNM67*(*Sma*I)	This study
pFS022	pRS414	*CNM67*::$(GA)_3$-*yEGFP1-6H*	This study
pFS024	pRS414	*CNM67*::$(GA)_3$-*3HA-6H*	This study
pFS048	pRS414	*CNM67*::$(GA)_{10}$-*3HA-6H*	This study
pFS025	pRS414	*cnm67*Δ*coil1*(*Sma*I)	This study
pFS026	pRS414	*cnm67*Δ*coil2*(*Sma*I)	This study
pFS027	pRS414	*cnm67*Δ*coil3*(*Sma*I)	This study
pFS028	pRS414	*cnm67*Δ*C*(*Sma*I)	This study
pFS029	pRS414	*cnm67*Δ*N*(*Sma*I)	This study
pFS030	pRS414	*cnm67*Δ*coil1*::$(GA)_3$-*yEGFP1-6H*	This study
pFS031	pRS414	*cnm67*Δ*coil2*::$(GA)_3$-*yEGFP1-6H*	This study
pFS032	pRS414	*cnm67*Δ*coil3*::$(GA)_3$-*yEGFP1-6H*	This study
pFS033	pRS414	*cnm67*Δ*C*::$(GA)_3$-*yEGFP1-6H*	This study
pFS034	pRS414	*cnm67*Δ*N*::$(GA)_3$-*yEGFP1-6H*	This study
pFS035	pRS414	*cnm67*Δ*coil1*::$(GA)_3$-*3HA-6H*	This study
pFS036	pRS414	*cnm67*Δ*coil2*::$(GA)_3$-*3HA-6H*	This study
pFS037	pRS414	*cnm67*Δ*coil3*::$(GA)_3$-*3HA-6H*	This study
pFS038	pRS414	*cnm67*Δ*C*::$(GA)_3$-*3HA-6H*	This study
pFS039	pRS414	*cnm67*Δ*N*::$(GA)_3$-*3HA-6H*	This study
pFS049	pRS414	*cnm67_Cterm*(*Sma*I)	This study
pFS089	pRS414	*cnm67_Cterm*::$(GA)_{10}$-*yEGFP1-6H*	This study
pFS090	pRS414	*cnm67_Nterm*::$(GA)_{10}$-*3HA-6H*	This study
pFS093	pRS414	*cnm67*Δ*coil1-3*(*Sma*I)	This study
pFS094	pRS414	*cnm67*Δ*coil1-3*::$(GA)_{10}$-*yEGFP1-6H*	This study
pFS095	pRS414	*cnm67*Δ*coil1-3*::$(GA)_{10}$-*3HA-6H*	This study
pFSC63	pUC19	*CNM67 (SmaI)*	This study
pFS103	pUC19	*cnm67_2coils*	This study
pFS105	pRS414	*cnm67_2coils*::$(GA)_{10}$-*yEGFP1-6H*	This study
pFS106	pRS414	*cnm67_2coils*::$(GA)_{10}$-*3HA-6H*	This study
pFS092	pRS414	*CNM67*::$(GA)_3$-*3HA-6H*::*HIS3MX6*	This study
pFS118	pRS414	*cnm67*Δ*C*::$(GA)_3$-*3HA-6H*::*HIS3MX6*	This study
pFS119	pRS414	*cnm67*Δ*N*::$(GA)_3$-*3HA-6H*::*HIS3MX6*	This study
pFS131	pRS414	*cnm67*Δ*coil1-3*::$(GA)_{10}$-*3HA-6H*::*HIS3MX6*	This study
pFS133	pRS414	*cnm67_2coils*::$(GA)_{10}$-*3HA-6H*::*HIS3MX6*	This study

The *CNM67* N-terminal fragment pFS090 was cloned by performing a PCR with divergent primers 5_R1 and GA7_F1 on pFS048, and the linear 6.2-kb fragment was circularized with T4 DNA ligase.

For deletion of all three coiled-coils to yield pFS093, an insert encompassing the C terminus and terminator of *CNM67* was brought in-frame by *Eco*RI cleavage of pFS027 and Klenow fill-in, released by *Bam*HI, and ligated into a vector part carrying only the fragment 5′ of the coil1 region. The latter was generated by cleaving pFS025 with *Nsi*I at the coil1 deletion site, blunting the *Nsi*I junction with Klenow in absence of dNTPs, and cutting out of the downstream fragment by *Bam*HI digestion. pFS094 and pFS095 tagged derivatives of pFS093 were constructed as described above.

pFS103 carrying a *cnm67* allele with doubled coil region was constructed as follows: wt *CNM67* was cloned *Kpn*I-*Bam*HI into pUC19 (Yanisch-Perron *et al*., 1985). A vector part consisting of *CNM67 coil region - CNM67 C terminus* - pUC19 vector backbone - *CNM67 N terminus* was amplified from pFS063 with the use of the primers DF5 and DR1, and the template DNA was destroyed with *Dpn*I. The entire coil region was amplified from pFS063 with the primer pair 2coil_F and 2coil_R, phosphorylated with PNK, and ligated into the vector part. The construct was cloned into pRS414 and tagged with a 3HA or yEGFP cassette as described above, yielding pFS105 and pFS106, respectively.

Integration cassettes with long flanking homologies to the *CNM67* genomic locus were constructed by transforming the plasmids pFS024, pFS038, pFS039, pFS095, and pFS106 carrying *CNM67* alleles into a yeast carrier strain, and PCR-targeting of the plasmid-borne *CNM67* terminator region with a *HIS3MX6* module (primers

MAF1 and MAR1). Isolation of plasmid DNA from HIS3$^+$ TRP1$^+$ transformants yielded the constructs pFS092, pFS118, pFS119, pFS131, and pFS133, respectively.

Protein Techniques

For total yeast protein extracts, ~4 × 10^8 log phase cells were collected, washed in ice-cold water, resuspended in 500 μl of cold TSNE lysis buffer (50 mM Tris-Cl pH 7.5, 150 mM NaCl, 1% [vol/vol] Nonidet-P40 [Fluka Chemie, Buchs, Switzerland], 1 mM EDTA) in presence of phosphatase inhibitors (10 mM Na-pyrophosphate, 10 mM β-glycerophosphate, 10 mM *p*-nitrophenyl-phosphate, 10 mM NaN_3, 10 mM NaF [Fluka Chemie]) and protease inhibitors (1 mM phenylmethylsulfonyl fluoride [Fluka Chemie], antipain, leupeptin, and pepstatin [Roche Diagnostics, Rotkreuz, Switzerland] at 1 μg/ml) and subjected to glass-bead lysis. Cell debris was removed by a short centrifugation step, and total protein concentration was determined by Bradford assay (Bio-Rad, Muenchen, Germany). Samples were adjusted for equalized load per gel lane, 2× FSB (125 mM Tris-Cl pH 6.8, 2% SDS, 0.1 M dithiothreitol, 30% [vol/vol] glycerol, 5% [vol/vol] β-mercaptoethanol) was added. The samples were boiled for 5 min and centrifuged for 5 min before loading onto the gel. SDS-PAGE for protein separation was performed as described (Laemmli, 1970) with the use of 10- × 14- × 0.15-cm 7.5% acrylamide gels. Western blotting was carried out according to Horvath and Riezman (1994), except for the use of 10% (wt/vol) dry milk and the addition of 0.1% (vol/vol) Nonidet P-40 for blocking and antibody incubations. Cnm67-3HAp was detected with mouse monoclonal anti-HA-Biotin 12CA5 (Roche Diagnostics) at a dilution of 0.8 μg/ml and visualized with the use of an enhanced chemiluminescence immunoblotting reagent kit (Amersham Pharmacia Biotech, Arlington Heights, IL).

Immunoprecipitation of Cnm67-3HAp was performed out of 800 μl of TSNE protein extracts (as described above) with 1 μg of rat monoclonal anti-HA high-affinity antibodies (clone 3F10; Roche Diagnostics) preadsorbed to 50 μl of gamma-G sepharose beads (Amersham Pharmacia Biotech, Uppsala, Sweden) for 2 h with gentle agitation at 4°C. The pellet was subjected to several washes in TSNE followed by washes in CIP buffer (50 mM Tris-CL pH 8.5, 5 mM $MgCl_2$), resuspended in 75 μl of CIP buffer, and split into 2 × 50 μl. Calf intestinal phosphatase (1 μl 10 U/μl; New England Biolabs), 10 mM β-glycerophosphate, and/or protease inhibitors were added as required, followed by a 15-min incubation at 37°C. The reactions were stopped by addition of 50 μl of 2× FSB and 5 min boiling, and the samples were analyzed by immunoblotting for Cnm67-3HAp as described above.

Microscopy

For nuclear migration assays, FSY020 cells carrying *cnm67* partial deletions on a plasmid were grown to an OD_{600} of 0.2–0.4 and mounted directly from growth medium onto poly-L-lysine-treated microscopy slides. Nuclear fluorescence of Histone H4-GFP (Hhf2-GFP) was observed through a fluorescein isothiocyanate-filter set, scoring cells containing one, two, or multiple nuclei. Total nuclear migration defect was calculated as the percentage of cells having more than one nucleus.

For colocalization of Cnm67-GFP with nuclei, FSY034 cells with plasmid-borne GFP-labeled *cnm67* mutants were grown to logarithmic phase, 5 μg/ml 4,6-diaminidino-2-phenylindole (DAPI) was directly added to the growth medium, and incubation at growth temperature was continued for 1 h. The cells were briefly washed, mounted for microscopy, and photographed immediately with the use of a video microscopy setup described in Brachat *et al.* (1998).

Electron Microscopy and Image Processing

Yeast cells were high-pressure frozen, freeze-substituted, and embedded according to the protocols described previously (Winey *et al.*, 1995) with the after modifications to improve the visibility of the SPB outer plaque. The freeze-substitution was done in acetone with 0.1% uranyl acetate and 2% osmium tetroxide before embedding in Spurr's resin. Sections were stained for 5 min with 2% uranyl acetate and 3 min with aqueous lead citrate.

SPB structural variations in wt, Δcoils, and 2coils mutants were measured from images of the SPBs. Electron microscopic images were captured digitally with a Gatan camera and Digital Micrograph software. A density profile of the SPB along the spindle axis was calculated with the use of the NIH Image software (developed at the U.S. National Institutes of Health and available on the Internet at http://rsb.info.nih.gov/nih-image/). The distance between the intermediate layer 2 (IL2), as defined in Bullitt *et al.* (1997) and O'Toole *et al.* (1999), and the outer plaque (OP) centers was determined by measuring the distance between the middle of the IL2 peak and the middle of the OP peak. The length of 20.3 nm for the coiled-coil element in Cnm67p was calculated according to the following formula:

$$\text{length} = [(\text{IL2-to-OP } \textit{CNM67}\_\text{wt} - \text{IL2-to-OP } \textit{cnm67}\_\Delta\textit{coils}) + (\text{IL2-to-OP } \textit{cnm67}\_\textit{2coils} - \text{IL2-to-OP } \textit{cnm67}\_\Delta\textit{coils})/2]/2 \quad (1)$$

The thickness of the outer plaque was measured at the 50% maximal pixel value of the OP peak's increasing and falling slopes. To take the altered outer plaque thickness of the mutants into consideration, the results were verified with the following formula:

$$\text{length} = [(\text{IL2-to-OP } \textit{CNM67}\_\text{wt} - \text{IL2 thickness}/2 - \text{OP thickness wt}/2) + (\text{IL2-to-OP } \textit{cnm67}\_\textit{2coils} - \text{IL2 thickness}/2 - \text{OP thickness 2coils}/2)/2]/2 \quad (2)$$

yielding an average of 19.7 nm. For this calculation, the gap between IL2 and OP in the *cnm67*Δ*coils* mutant was assumed to be zero, because no gap is seen the corresponding density plots.

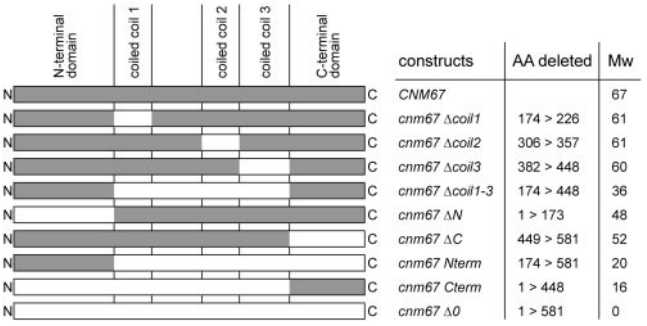

constructs	AA deleted	Mw
CNM67		67
cnm67 Δcoil1	174 > 226	61
cnm67 Δcoil2	306 > 357	61
cnm67 Δcoil3	382 > 448	60
cnm67 Δcoil1-3	174 > 448	36
cnm67 ΔN	1 > 173	48
cnm67 ΔC	449 > 581	52
cnm67 Nterm	174 > 581	20
cnm67 Cterm	1 > 448	16
cnm67 Δ0	1 > 581	0

Figure 1. Overview of the PCR-generated *cnm67* partial deletions. The breakpoints between the domains were determined with the paircoils program as described in Brachat *et al.* (1998); Figure 2A). In addition, all plasmid constructs carry a *Sma*I site before the STOP codon for tag cassette insertion (see MATERIALS AND METHODS). *cnm67 Δ0* corresponds to the empty pRS414 vector transformed into a *cnm67*Δ deletion strain background. AA deleted, amino acids deleted; Mw, predicted molecular weight.

RESULTS

Analysis of CNM67 Partial Deletions Reveals Two Domains Important for Nuclear Migration Function

Analysis of the Cnm67p peptide revealed three separate regions with high coiled-coil formation potential in the cen-

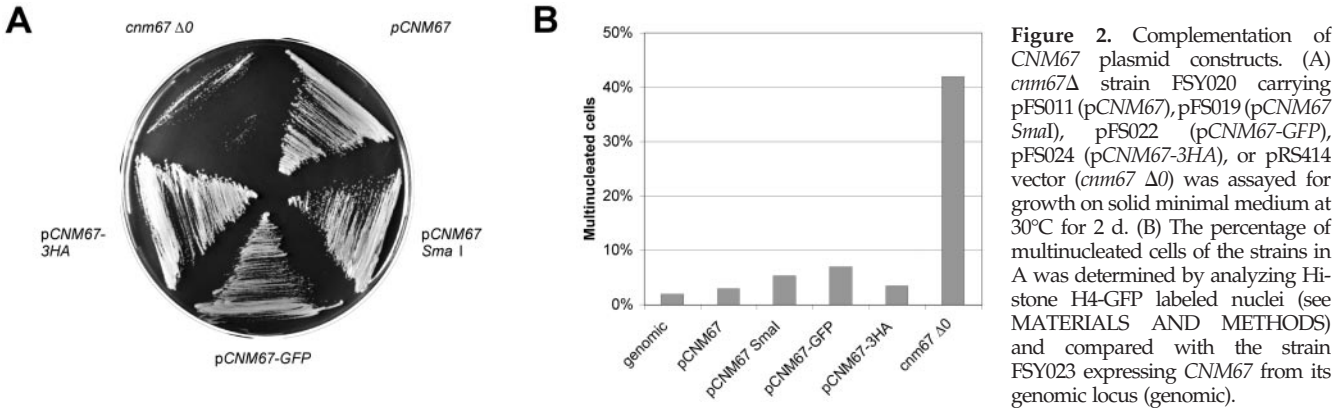

Figure 2. Complementation of *CNM67* plasmid constructs. (A) *cnm67*Δ strain FSY020 carrying pFS011 (p*CNM67*), pFS019 (p*CNM67 Sma*I), pFS022 (p*CNM67-GFP*), pFS024 (p*CNM67-3HA*), or pRS414 vector (*cnm67* Δ*0*) was assayed for growth on solid minimal medium at 30°C for 2 d. (B) The percentage of multinucleated cells of the strains in A was determined by analyzing Histone H4-GFP labeled nuclei (see MATERIALS AND METHODS) and compared with the strain FSY023 expressing *CNM67* from its genomic locus (genomic).

ter of the sequence, flanked by an N-terminal and a C-terminal globular domain (Brachat *et al.*, 1998), whereas other functional domains where not found. To dissect the function of Cnm67p at the SPB, precise deletions of single and multiple domains were carried out by PCR as illustrated in Figure 1 (see MATERIALS AND METHODS). FSY020, a *cnm67*Δ strain that carries a Histone H4-GFP marker as a nuclear label, and FSY034 as its unlabeled, but otherwise isogenic derivative, were used to test functionality of the altered *CNM67* genes, including complementation of *cnm67*Δ. Previously, cells deleted for *CNM67* were shown to have a severe nuclear migration defect, which resulted in a slow growth phenotype (Brachat *et al.*, 1998). With a plasmid carrying wt *CNM67* (Figure 2, p*CNM67*) both, slow growth and nuclear missegregation are successfully complemented to levels of genomically expressed *CNM67* (Figure 2B, genomic). Neither the construction of a *Sma*I cloning site immediately 5′ of the *CNM67* STOP codon, nor the insertion of *GFP* or *3HA* cassettes into this *Sma*I site significantly affects the complementation capacity of the constructs (Figure 2, p*CNM67 Sma*I, p*CNM67-GFP*, p*CNM67-3HA*). In all cases, normal growth on solid medium (Figure 2A) correlates with successful nuclear migration (Figure 2B). Identical results were obtained for FSY034 (our unpublished results), demonstrating that the H4-GFP label has no effect on nuclear migration fidelity. From these data, we conclude that C-terminal tagging of *CNM67* does not have an effect on the functionality of the protein in nuclear migration.

In a first step, the growth of *CNM67* partial deletion strains on solid medium was examined because slow growth was shown to be indicative of loss of *CNM67* function (Figure 2). Severe growth defects are observed in *cnm67* mutants lacking the N or C terminus of the protein (Figure 3A, *cnm67* Δ*N* and *cnm67* Δ*C*). However, the deletion of single coiled regions (Figure 3A, *cnm67* Δ*coil1*, *cnm67* Δ*coil2*, and *cnm67* Δ*coil3*), or the entire coiled region (Figure 3A, *cnm67* Δ*coil1-3*) does not significantly impair growth. We then wanted to determine whether the slow growth phenotype of cells expressing *cnm67* lacking either the N or C terminus could be correlated with a defect in nuclear migration as observed for the complete deletion of *CNM67* (Figure 2). To do so, *cnm67*Δ cells coexpressing the various partial deletions of *CNM67* with *HHF2-GFP* to visualize the nuclei were grown in liquid medium and prepared for microscopy. Representative images of cells carrying the various partial deletions are shown in Figure 3B. A high incidence of multinucleated cells (40% or greater, Figure 3C) similar to the null strain can be observed in the samples from strains carrying N- or C-terminally deleted *CNM67*. In contrast, mutations in the coil region led to a relatively mild phenotype (15% multinucleated cells or less, Figure 3C). Interestingly, one-third of the protein can be deleted by removing the entire coiled-coil region without producing a drastic increase in bi- and multinucleated cells (Figures 3B, *cnm67* Δ*coil1-3*, and C). For all partial deletion mutants, the slow growth phenotype correlates with the failure to undergo correct nuclear migration.

C Terminus of Cnm67p Carries a Determinant Important for SPB Localization

Cnm67-GFP is known to localize to the SPBs (Brachat *et al.*, 1998). We wanted to elucidate which part of the protein is responsible for localizing Cnm67p to the SPB by making use of our partial deletion constructs. Strains containing *cnm67*Δ and expressing either wild-type Cnm67-GFP or GFP-tagged partial deletions of Cnm67p were grown in liquid medium and DNA was stained with DAPI to allow colocalization of the GFP signal and the nuclei. Fluorescence micrographs of these cells are shown in Figure 4. As expected, plasmid-encoded wild-type Cnm67-GFP is found to localize at SPBs at the periphery of the DAPI-stained DNA mass (Figure 4, *CNM67*). Cnm67p lacking the N terminus (Figure 4, *cnm67* Δ*N*), coils1, 2, or 3, or even the entire coil domain (Figure 4, *cnm67* Δ*coil1*, *cnm67* Δ*coil2*, *cnm67* Δ*coil3*, or *cnm67* Δ*coil1-3*) still localize to the SPB region on the nuclear periphery. The GFP signal is also detected on all the nuclei in the multinucleated cells present in several panels of Figure 4. In contrast, cells carrying a C-terminally deleted *cnm67*Δ*C* exhibit no SPB signal in any cell examined (Figure 4, *cnm67* Δ*C*), even although the mutant protein is expressed at levels comparable to wt Cnm67p (Figure 5B). The C terminus of Cnm67p alone, however, is not sufficient to localize to the SPB (Figure 4, *cnm67* Cterm), although it too is expressed (our unpublished results). These observations were confirmed by repeating the experiment with the use of a highly sensitive cooled charge-coupled device camera.

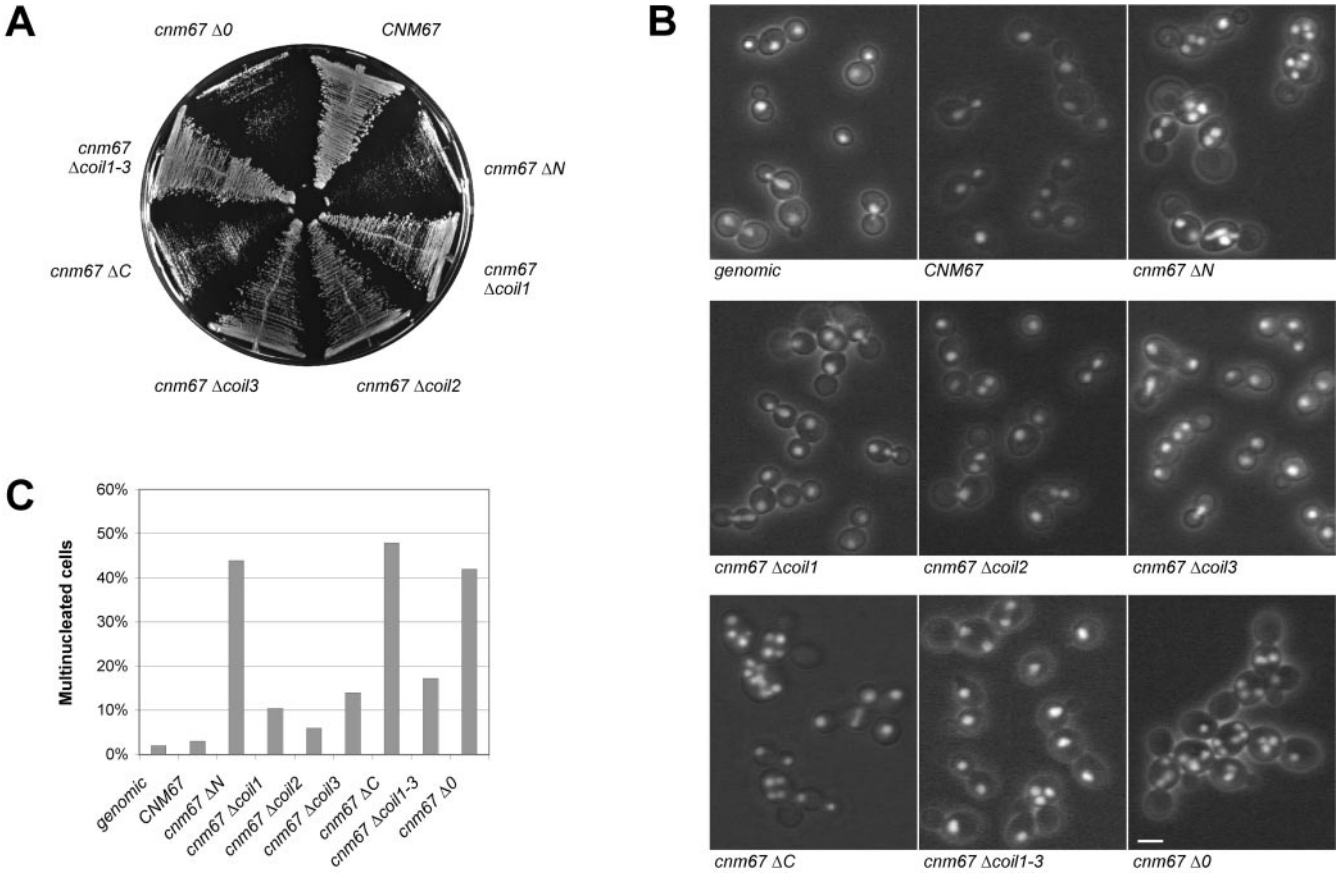

Figure 3. Effects of *cnm67* partial deletions on growth and nuclear migration fidelity. FSY020 carrying a genomic deletion of *CNM67* was transformed with pFS019 (*CNM67*), pFS029 (*cnm67 ΔN), pFS025 (*cnm67 Δcoil1), pFS026 (*cnm67 Δcoil2), pFS027 (*cnm67 Δcoil3), pFS028 (*cnm67 ΔC), pFS093 (*cnm67 Δcoil1–3), and with pRS414 (*cnm67 Δ0*) as vector control. FSY023 carrying wt *CNM67* on its genomic locus was used as the isogenic control strain in B and C. (A) Strains described above were assayed for growth on solid minimal medium for 2 d at 30°C. (B) Representative micrographs of the aforementioned strains grown selectively in liquid medium at 30°C overnight and directly prepared for microscopy (see MATERIALS AND METHODS). The cells were visualized with combined phase contrast and fluorescein isothiocyanate fluorescence filters to detect the cell shape and the nuclear fluorescence signal of *Histone H4-GFP*. Bar, 5 μm. (C) The number of nuclei per cell was determined and the nuclear migration defects plotted as the percentage of cells containing more than one nucleus (n > 200).

Cnm67p Is Phosphorylated within the N-Terminal Domain

Many structural components of the *S. cerevisiae* SPB are known to be phosphorylated (Donaldson and Kilmartin, 1996; Friedman *et al.*, 1996; Stirling and Stark, 1996; Knop *et al.*, 1997; Pereira *et al.*, 1998, 1999; Wigge *et al.*, 1998; Gruneberg *et al.*, 2000). To elucidate whether this is also true for the outer plaque component Cnm67p, we first tested the protein for phosphorylation. Immunoblot analysis of protein lysates prepared from logarithmically growing wild-type cells carrying a genomically tagged *CNM67-3HA* allele reveals several electrophoretically distinct forms of the protein (Figure 5A, lane total extract). To assess the nature of the observed variation in electrophoretic mobility, Cnm67p was immunoprecipitated from an extract of logarithmically growing cells (Figure 5A, lane total extract, lane sup) and subjected to phosphatase treatment. The modified forms of purified Cnm67p were not altered by incubation at 37°C (Figure 5A, lane −CIP), showing that no endogenous phosphatase or protease activities were coprecipitated. However, all slow-migrating variants of Cnm67p are converted to the 67-kDa form upon dephosphorylation (Figure 5A, lane +CIP). This conversion is inhibited by β-glycerophosphate, a phosphatase-specific inhibitor (Figure 5A, lane +CIP + 3GP). Furthermore, addition of protease inhibitors with active phosphatase (Figure 5A, lane +CIP +Pi) does not prevent the conversion, and addition of protease inhibitors with phosphatase inhibitors (Figure 5A, lane +CIP + 3GP +Pi) does not result in disappearance of the slowly migrating species. This demonstrates that the conversion in electrophoretic mobility observed upon CIP treatment is due to the phosphatase activity, and not to proteolytic contaminations of the CIP preparation. In conclusion, the data show that Cnm67p is posttranslationally modified by phosphorylation. Thus, in all subsequent analyses the shift in SDS-PAGE mobility of Cnm67p is used as an indicator of its phosphorylation state.

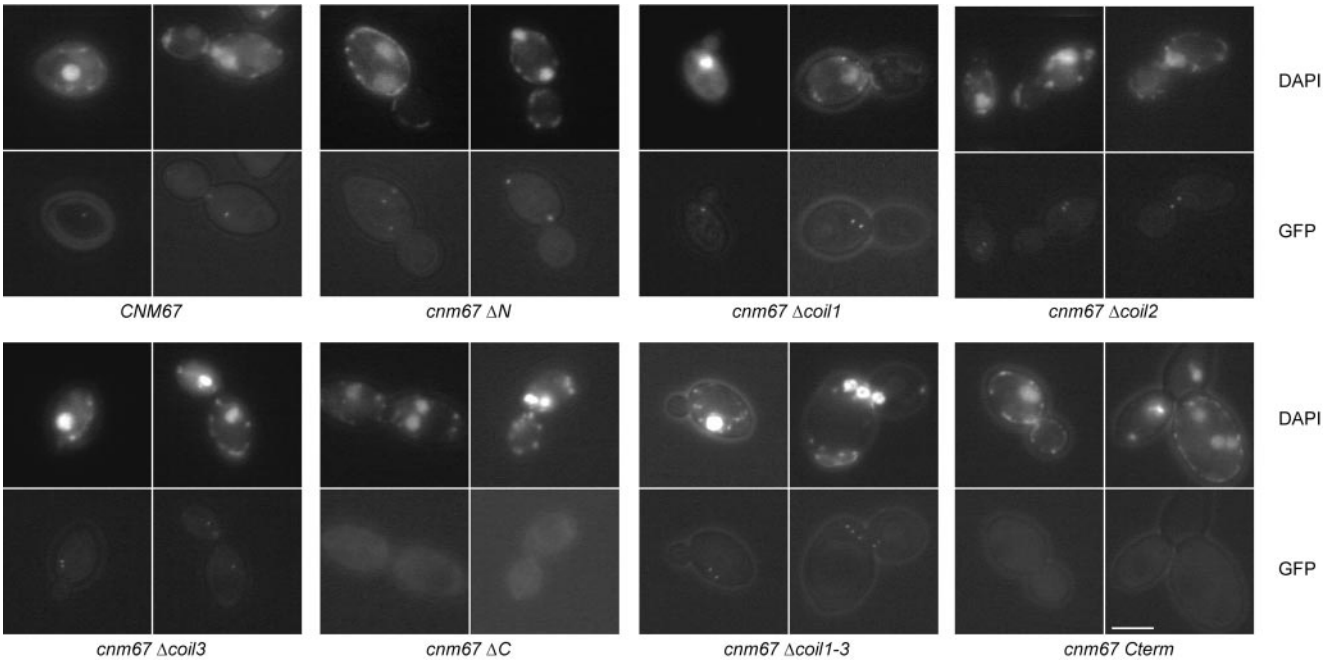

Figure 4. Localization of Cnm67p partial deletions to the spindle pole body region. The *cnm67*Δ strain FSY034 was transformed with the GFP-tagged *cnm67* partial deletion plasmids pFS022 (*CNM67*), pFS034 (*cnm67*Δ*N*), pFS030 (*cnm67* Δ*coil1), pFS031 (*cnm67 Δcoil2), pFS032 (*cnm67* Δ*coil3), pFS033 (*cnm67 ΔC), pFS094 (*cnm67* Δ*coil1-3*), and with pFS089 (*cnm67 Cterm*). The strains were grown in liquid minimal medium at 30°C overnight. DNA was stained by adding DAPI to the growth medium for 1 h. Cells were then examined by epifluorescence to visualize the GFP and DAPI signals. Bar, 5 μm.

We next wanted to determine whether the phosphorylation of Cnm67p could be mapped to a single domain, and to determine whether lack of SPB localization of the protein influences its phosphorylation state. The phosphorylation state of 3HA-tagged *cnm67* partial deletions was analyzed by immunoprecipitation from protein extracts of logarithmi-

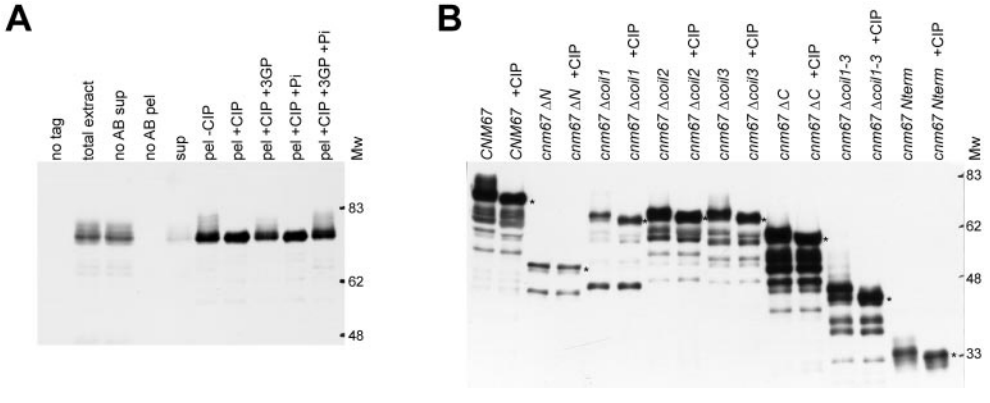

Figure 5. Cnm67p is phosphorylated within its N-terminal domain. (A) Multiple species in SDS-PAGE mobility is due to phosphorylation of Cnm67p. Cells expressing Cnm67-3HAp (ABY132) were grown in YPD to logarithmic phase, total protein extracts were prepared, and Cnm67-3HAp was immunoprecipitated (IP) and detected with anti-HA antibodies as described in MATERIALS AND METHODS. Samples loaded on the gel were prepared as follows: no tag, total protein extract of an untagged strain (CEN. PK2) as a control for the specificity of the detection antibody; total extract, total extract of a Cnm67-3HAp tagged strain; no AB sup and no AB pel, control IP carried out without antibody to demonstrate the specificity of the immunoprecipitation; sup, IP supernatant; pel −CIP, IP pellet incubated at 37°C for 15 min without CIP; pel +CIP, pellet incubated with 10 U of CIP; pel +CIP +3GP, addition of CIP and β-glycerophosphate as inhibitor; pel +CIP +Pi, addition of CIP and protease inhibitors; pel +CIP +3GP +Pi, addition of CIP, β-glycerophosphate, and protease inhibitors. (B) Phosphorylation state of Cnm67p partial deletion proteins. *cnm67*Δ cells FSY020 were transformed with either C terminally 3HA-tagged wt *CNM67* (pFS024) or with *cnm67* partial deletion plasmids, *cnm67* Δ*N (pFS039),* cnm67 Δcoil1 (pFS035), *cnm67* Δ*coil2 (pFS036),* cnm67 Δcoil3 (pFS037), *cnm67* Δ*C (pFS038),* cnm67 Δcoil1-3 (pFS095), and with *cnm67 Nterm* (pFS090). Protein extracts from logarithmically growing cultures were prepared, Cnm67-3HAp purified by immunoprecipitation, incubated with (+CIP lanes) or without (−CIP lanes) phosphatase, and immunodetected. Protein degradation observed in this experiment was found to be an effect of the growth in minimal medium and not a consequence of the mutated alleles themselves (our unpublished results). Asterisks mark the location of the nonphosphorylated, undegraded protein.

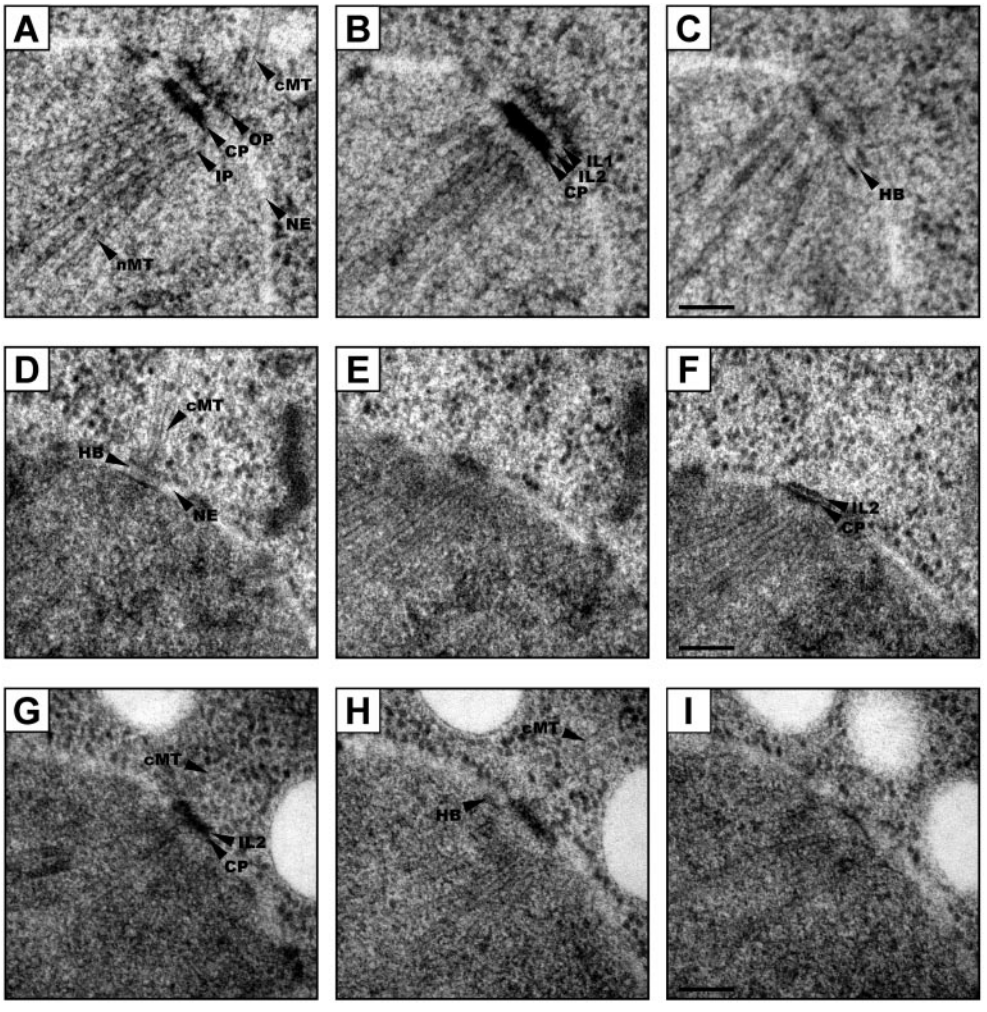

Figure 6. Deletion of the N or C terminus of Cnm67p prevents formation of a functional outer plaque structure. Elements of the images are labeled as nMT, nuclear microtubules; IP, inner plaque; CP, central plaque; NE, nuclear envelope; IL2, intermediate layer 2; IL1, intermediate layer 1; OP, outer plaque; cMT, cytoplasmic microtubules; HB, half bridge. Bar, 100 nm. (A–C) Serial sections of a *CNM67* cell (FSY170) having established a bipolar spindle. Nucleation of cMTs occurs at the outer plaque. (D–F) Outer plaques were not detectable in serial sections of *cnm67* Δ*N* (FSY175) SPBs. In absence of this structure, cytoplasmic microtubules are found attached to the half bridge, as well as at SPB on rare occasion. The half-bridge itself lies above the SPB plane (E and F) and therefore appeared in a separate section (D) as two electron-dense layers on the nuclear envelope. (G–I) Serial section of a *cnm67* Δ*C* (FSY174) SPB. In this mutant, the outer plaque was not detected in any section examined. Cytoplasmic microtubules were leading to the half-bridge region on the left side of the SPB (G and H).

cally growing strains carrying 3HA-tagged partial deletions of *cnm67*. The presence of phosphorylation on the immunoprecipitated mutant proteins was then assayed by comparing phosphatase-treated and nontreated samples by immunoblot (Figure 5B). 3HA-tagged *CNM67* full-length protein expressed from a CEN/ARS plasmid (Figure 5B, lanes *CNM67*) shows a pattern identical to genomically tagged *CNM67* (compare Figure 5A). Proteins encoded by all but the N-terminal deletion constructs show a phosphorylation pattern, including several slow-migrating isoforms that are converted to the fast-migrating band (Figure 5B, asterisk) by dephosphorylation. Mislocalization as observed with the *cnm67* Δ*C* mutant protein does not prevent phosphorylation (Figure 5B, lanes *cnm67* Δ*C*). In cells expressing the N-terminal truncation, a single band migrating at the expected molecular weight of 53 kDa (48 kDa + 5-kDa tag) is seen that is unaffected by phosphatase treatment (Figure 5B, lanes *cnm67* Δ*N*). Expression of the Cnm67p N terminus alone resulted in a series of bands at ~33 kDa that clearly migrated faster upon incubation with phosphatase (Figure 5B, lanes *cnm67 Nterm*). Thus, the Cnm67p N terminus is necessary and sufficient for phosphorylation to occur.

Taken together, our observations indicate that functions likely to be important for Cnm67p's role in nuclear migration, localization to the SPB and phosphorylation, are concentrated in the C- and N-terminal regions, respectively, of the Cnm67 polypeptide chain.

Cnm67p N- and C-Terminal Truncations Both Result in Loss of SPB Outer Plaque

To determine whether the failure to undergo correct nuclear migration in cells carrying *cnm67* partial deletions stems from a common origin, we set out to analyze the fine structure of the SPBs of these mutants by electron microscopy. Partial deletions of *CNM67* were integrated at their genomic locus under the control of their original promoter (see MATERIALS AND METHODS). To retain the structure of the associated proteins and the interaction with microtubules, in situ visualization of the SPB by electron microscopy was performed on serial thin sections of fast-frozen and freeze-substituted cells (Winey *et al.*, 1995; see MATERIALS AND METHODS). This method has yielded excellent conservation of the SPB vertical architecture (O'Toole *et al.*, 1999).

Micrographs of SPBs in serial sections of cells carrying the wild-type *CNM67* integration construct are shown in Figure 6, A–C. According to the nomenclature of Bullitt *et al.* (1997), the multilaminar SPB structure can be divided into six major electron-dense layers. These include the inner plaque (IP) with a separate layer of the nuclear, or spindle, microtubule ends (nMT); the central plaque (CP) at the level of the nuclear envelope (NE); the intermediate layer 2 (IL2), with a smaller diameter situated on top of the CP; the intermediate layer 1 (IL1) sometimes visible as vertical striations connecting IL2 and OP (Figure 6B); and the outer plaque (OP) nucleating the cytoplasmic, or astral, microtubules (cMT). In contrast to glutaraldehyde-fixed SPBs where IL2 and CP usually appear to be fused, the freeze-substituted preparation allows a clear resolution of the two separate layers. In all 20 wt SPBs examined, the outer plaque is present, and 13 of these 20 have cMTs emanating from the outer plaque. For the remaining seven SPBs, the origin of cMTs could not be assigned (two cases) or no microtubules could be detected (five cases). This could be explained by the fact that detection of cMTs by thin section electron microscopy is technically difficult, because there are only few such microtubules per SPB and, unlike nuclear microtubules, cMTs emerge from the SPB at many different angles. Consistent with Byers and Goetsch (1975), cMTs at the half bridge were only detected in cells having duplicated the SPB, but not having separated the SPBs to establish a bipolar spindle. This was the case in one of 20 SPBs inspected, where these microtubules were detected in addition to the outer plaque microtubules.

We next analyzed the N-terminal deletion mutant for alterations in the SPB structure. This mutant protein was expected to be present at the SPB (Figure 4). Representative micrographs are shown in Figure 6, D–F. As anticipated from the nuclear migration defect of this allele (Figure 3), the outer plaque cannot be detected on any of the 12 SPBs examined. In three cases, cMTs appear to be at the SPB itself, whereas cMTs were found to originate from the half bridge structure on three other SPBs (Figure 6D). For three SPBs, the origin of the microtubules was uncertain partially because the cMTs appear to be parallel to the SPB, and in three cases no cMTs were detected. The possibility that the half bridge can be located above or below the sectioning plane, as illustrated in Figure 6D, might have contributed to the number of microtubules having an undefined origin.

Cnm67p deleted for its C terminus was shown not to localize to the SPB (Figure 4). For this allele, we expected severe structural defects in the SPB outer plaque that are confirmed by our finding that the outer plaque is missing from all 25 SPBs analyzed (Figure 6, G–I). In this mutant, it was particularly difficult to detect cytoplasmic microtubules. We determined that five SPBs displayed an attachment of cMTs to the half bridge, whereas in seven situations, the cMT origin could not be assigned. Finally, no cMTs were found at the 13 remaining SPBs.

Because SPBs in cells containing either the *cnm67* Δ*N* or the *cnm67* Δ*C* allele are devoid of the outer plaque structure, we wanted to determine whether the difference in Cnm67p localization to the SPB would be reflected by a change in the substructures remaining at the SPB. Comparing SPBs of the aforementioned mutants reveals no structure that could be representative of Cnm67 protein. This observation is most likely explained by the fact that the staining of the IL1 generally is weak, such that the presence or absence of Cnm67p cannot be assessed.

In summary, both N- and C-terminal deletion mutants of Cnm67p exhibit severe defects in the SPB outer plaque region. Cytoplasmic (astral) MTs in these mutants are predominantly found on the half bridge, but in some cases the cMTs run parallel to the SPB making their origin difficult to determine and in very few cases with the N-terminal deletion of Cnm67p the cMTs are found at the SPB.

Cnm67p Is a Spacer on Cytoplasmic Face of Spindle Pole Body

Considering the SPB defects observed in cells harboring the N- and C-terminal partial deletions of *CNM67*, one could speculate that deletions in the coil region that only cause a mild nuclear missegregation phenotype would result in more subtle structural changes. We tested this idea by comparing micrographs of SPBs from cells carrying a deletion of all three coils (Figure 7, A–C) to those from cells with wild-type *CNM67* (Figure 6, A–C). As expected, the SPB integrity of the *cnm67*-Δ*coils* containing cells is not affected. Outer plaque structures are easily detected on 10 of 11 SPBs examined in cells carrying the *cnm67*-Δ*coils* allele, and in more than half of the cases the outer plaque is associated with cMTs. Nevertheless, the orderly assembly of the outer plaque appears to be disturbed. Five of the 10 SPBs were found to display clustering or discontinuities in the density of the outer plaque material (Figure 7C), such that outer plaques have a diffuse appearance and do not reach the lateral size of the IL2. The cases with disturbed outer plaque structure, however, did not significantly coincide with the presence or absence of cMTs.

We also noticed that the gap between IL2 and the outer plaque in the *cnm67* Δ*coils* mutants cells was significantly reduced compared with wild-type cells. This observation, along with recent two-hybrid data (Adams and Kilmartin, 1999; Elliott *et al.*, 1999), gave rise to the hypothesis that Cnm67p could be a spacer protein between the central and outer plaque, similar to Spc110p on the nuclear side of the SPB (Kilmartin *et al.*, 1993). To test this hypothesis, a *cnm67* allele with a tandem-repeat of the coil region (*cnm67 2coils*) was constructed. With the use of a GFP-tagged variant of the construct, correct localization to the SPB region was demonstrated as seen by localization to the edge of the DAPI-stained nuclear DNA (Figure 7, H and I). The overall structural integrity of the SPB is not disturbed by the mutation (Figure 7, D–F). In some cases, thicker outer plaques are observed, but binding of cMTs seems not to be affected (Figure 7G). This is also reflected by the fact that cells relying on *cnm67 2coils* as the sole source of Cnm67p achieve nuclear migration with wild-type fidelity (our unpublished results).

Comparison of wild-type SPBs with those in strains containing *cnm67* Δ*coils* and *cnm67 2coils* reveals obvious differences in the distance of the outer plaque to the electron-dense IL2 (Figure 8A). The spacing varied by roughly 20 nm upon deletion or addition of a complete set of coiled-coil domains. Statistical evaluation of the distances between the centers of the IL2 and the outer plaque electron density reveals a significant decrease from 40.5 nm in wt ($n = 17$, $\sigma = 3.7$) to 18 nm ($n = 9$, $\sigma = 2.7$) in the *cnm67* Δ*coils* mutant, and an increase from 40.5 to 55.4 nm ($n = 11$, $\sigma = 4.8$) upon doubling of the coiled-coil region in the *cnm67 2coils* mutant

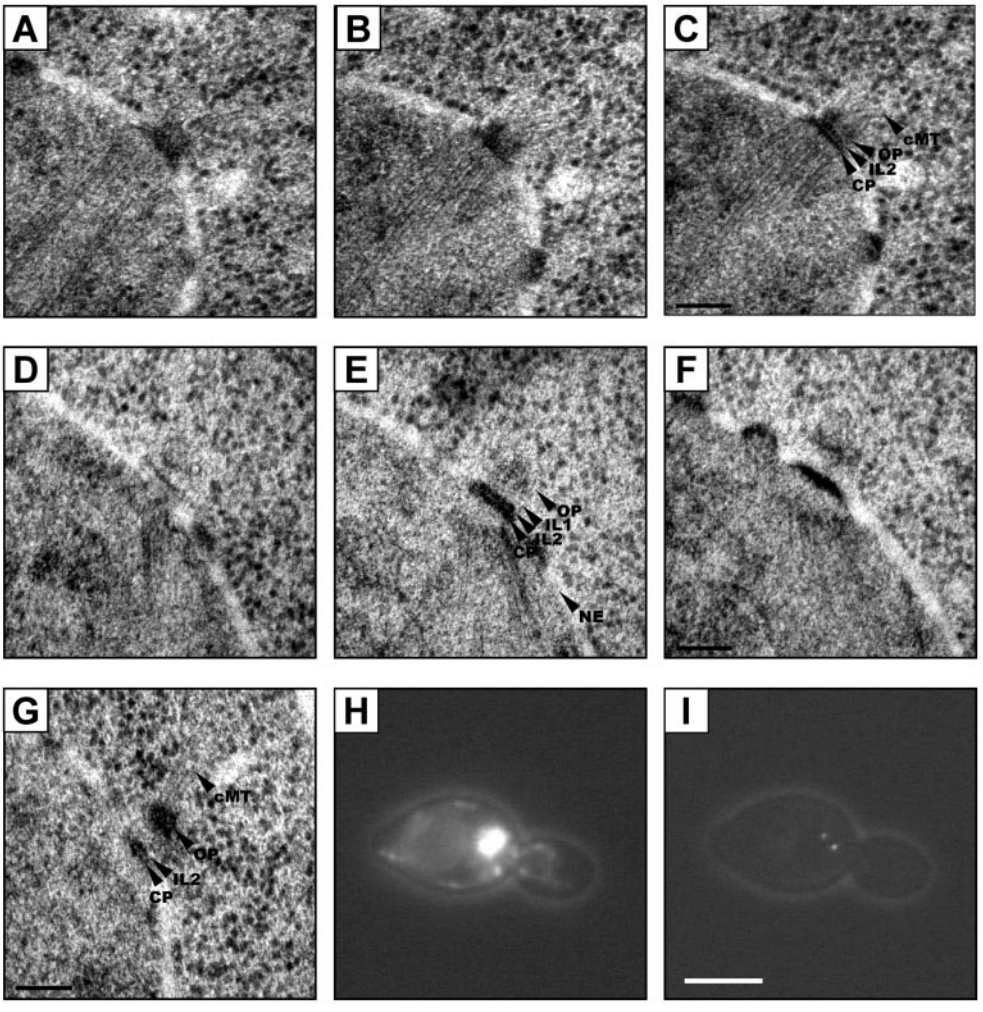

Figure 7. Mutations in the central coil region of Cnm67p affect the IL1 structure. Elements of the images are labeled as CP, central plaque; IL2, intermediate layer 2; IL1, intermediate layer 1; OP, outer plaque; cMT, cytoplasmic microtubules. (A–C) Serial sections of the *cnm67* Δ*coils* mutant (FSY182). In contrast to *cnm67* ΔN and *cnm67* ΔC deletion of the coil region did not abolish the outer plaque, and the structure was capable of nucleating cMTs. The outer plaque in this example exhibits an uneven density, with a concentration of material at the edges (C). In contrast to wild type, the IL1 gap was not detected. Bar, 100 nm. (D–F) Serial sections of a *cnm67 2coils* (FSY184) SPB. Doubling of the coiled-coil region resulted in a wider gap at the level of intermediate layer 1. Bar, 100 nm. (G) An increase in outer plaque vertical dimension was observed in *cnm67 2coils* cells. Bar, 100 nm. (H–I) Cnm67 2coils protein localizes to the SPB region on the nuclear periphery. (H) DAPI nuclear staining. (I) Cnm67 2coils-GFP. Bar, 5 μm.

(Figure 8B). Along with an extended gap between IL2 and outer plaque, a slight increase in plaque thickness is observed in cells carrying the elongated Cnm67 2coils protein (Figures 7G and 8C). To exclude any influence upon the accuracy of the measurements, the IL2-to-outer plaque distances were verified taking the altered outer plaque thickness into consideration (see MATERIALS AND METHODS).

In summary, these results suggest that Cnm67p is a spacer protein on the cytoplasmic face of the SPB, whose coiled-coil domain determines the distance between the electron-dense intermediate layer 2 and the outer plaque.

DISCUSSION

Cnm67p N- and C-Terminal Domains Have Distinct Functions

CNM67 was discovered as a gene important for the formation of the SPB outer plaque, and thus for successful nuclear migration via cytoplasmic microtubules attached to the outer plaque (Brachat *et al.*, 1998). Analysis of Cnm67p revealed regions with high coiled-coil formation potential (Brachat *et al.*, 1998), a feature shared by many structural components of the SPB (Kilmartin *et al.*, 1993; Knop and Schiebel, 1998; Mirzayan *et al.*, 1992; Souès and Adams, 1998). We have shown that the N- and C-terminal domains of Cnm67p are important for its function at the SPB by analyzing the nuclear migration fidelity of cells carrying partial deletions in *CNM67* (Figure 3). Coiled-coil domains are generally believed to play a role in homo-oligomerization or association into complexes with other proteins (Lupas, 1996; Newman *et al.*, 2000). In the case of Cnm67p, this function, although probable according to two-hybrid data (Elliott *et al.*, 1999), seems to be secondary in terms of the protein's function in nuclear migration, because deletion of the entire coiled-coil region only results in a moderate phenotype.

Localization of the Cnm67p to the SPB was specifically abolished by deletion of its C-terminal domain. This domain alone, however, was not sufficient to locate to the SPB (Figure 4). As all other deletions in the protein did not affect SPB localization, we suggest that the C terminus is acting as a SPB anchor and/or targeting domain. But because the C terminus is not sufficient for SPB localization, Cnm67p probably requires accessory factors interacting with the other

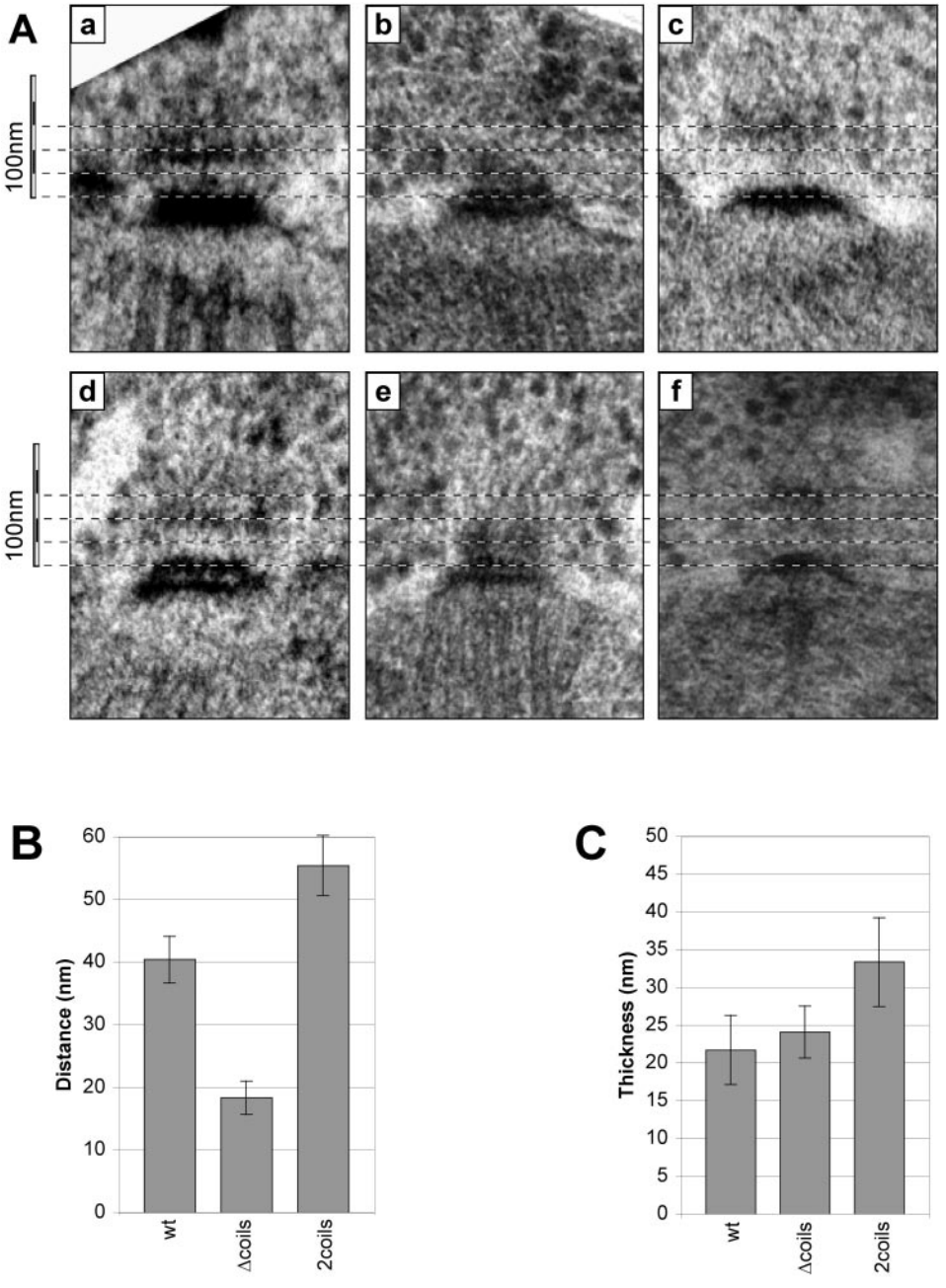

Figure 8. Cnm67p acts as a spacer between intermediate layer 2 and the outer plaque. (A) Visual comparison of the variations in the IL2-to-outer plaque distance of the coiled-coil mutants. Two independent series of SPBs are shown in a–c and d–f. The SPBs were aligned with their IL2 (bottom line) and the middle of the outer plaques were marked (top three lines). a and d represent wild-type SPBs, b and e are *cnm67* Δ*coils* SPBs, and c and f are SPBs of *cnm67 2coils* cells. The scale subdivisions correspond to 20 nm units. (B) Statistical evaluation of the IL2-to-outer plaque distances. The columns represent the average distance between the centers of the IL2 and outer plaque, measured on SPB density profiles along the spindle axis; the error bars mark the standard deviation σ (see text). (C) Thickness of *CNM67, cnm67* Δ*coils*, and *cnm67 2coils* mutants' outer plaques were measured on SPB density plots; σ is represented by the error bars.

domains to target Cnm67p to the SPB. We can also conclude that localization to the SPB is essential for its function in nuclear migration and, therefore, required for normal growth. The idea that Cnm67p is anchored to the SPB by its C terminus is also supported by two reports of two-hybrid interactions between the central plaque component Spc42p and the Cnm67p C terminus (Adams and Kilmartin, 1999; Elliott *et al*., 1999).

We have shown that Cnm67p is a phosphoprotein by immunoprecipitation and subsequent phosphatase treatment. With the use of the partial deletion constructs, we mapped the region of phosphorylation to the N-terminal part of the protein (Figure 5B). Analysis of N-terminal degradation products suggests that a part of the phosphorylation sites is located within the first 7 kDa of the polypeptide chain. Removal of the coiled-coils or C-terminal regions of Cnm67p did not affect phosphorylation of the protein. We expressed the N-terminal domain alone and were able to detect a series of phosphorylated isoforms, demonstrating that the N terminus harbors the sites of phosphorylation. These findings show that the Cnm67p N terminus is necessary and sufficient for phosphorylation to occur. Intriguingly, mislocalization of Cnm67p, as it occurs with a C-terminal deletion allele, did not abrogate phosphorylation.

Therefore, correct localization of Cnm67 is not necessarily a prerequisite for phosphorylation to take place. Recently, evidence is accumulating that phosphorylation of outer plaque components might play a role in regulation of cMT attachment to the outer plaque (Gruneberg *et al.*, 2000). Whether phosphorylation of the Cnm67p N terminus, located proximal to the outer plaque, is involved in this process, currently is under investigation.

Presence of Spindle Pole Body Outer Plaque Is Dependent on N and C Terminus of Cnm67p

We have shown that deletion of the N- or C-terminal domain of Cnm67p has deleterious effects on nuclear migration fidelity. Deletion of the central coiled-coil domain, however, only has mild effects on nuclear migration. Fine-structural analysis with the use of electron microscopy revealed that the basis of the nuclear missegregation in *cnm67* Δ*N* and *cnm67* Δ*C* cells was a severe defect of the outer plaque region of the SPB. In absence of a functional outer plaque, the only site for cytoplasmic microtubule attachment is the half-bridge (Brachat *et al.*, 1998). Compared with wild-type, where MT attachment to the half-bridge is restricted to a narrow time window in the G1 phase of the cell cycle (Byers and Goetsch, 1975), cells carrying the ΔN or ΔC alleles displayed cytoplasmic microtubules emanating from the half-bridge throughout the cell cycle. Similar to the *cnm67* null mutant (Brachat *et al.*, 1998), these microtubules provide a rescue pathway that allows for inefficient nuclear migration to occur. Recent dynamic studies of cytoplasmic microtubules in a *cnm67*Δ mutant, revealed detachment of cytoplasmic MT after SPB separation (Hoepfner *et al.*, 2000), suggesting that there is destabilization of microtubule attachment to the half-bridge upon establishment of a bipolar spindle. This, together with our observation that only a fraction of the SPBs in *cnm67* Δ*N* or *cnm67* Δ*C* strains display MTs anchored at the half-bridge may, in turn, be the reason for the low efficiency of this rescue pathway.

Our data suggest that the anchoring of the structural proteins required for the formation of the outer plaque is dependent on the presence of Cnm67p at the cytoplasmic face of the SPB. This activity requires both the C terminus and the N-terminal domain. Although the detection of a layer representing the Cnm67 protein itself was not possible, several other lines of evidence together with our results support the idea of Cnm67p being a linker element between IL2 and structures of the outer plaque. First, Cnm67p was localized exclusively to the SPB itself, but not to the half-bridge (Wigge *et al.*, 1998; Adams and Kilmartin, 1999). Second, two-hybrid interactions were found between the Cnm67p C terminus and the Spc42p C terminus of the IL2 region, and between the Cnm67p N terminus and Spc94/Nud1 of the outer plaque (Elliott *et al.*, 1999). Finally, components of the outer plaque, Spc94p/Nud1p and Spc72p, are relocalized from the SPB to the half-bridge upon deletion of *CNM67* (Adams and Kilmartin, 1999).

Previously, we have shown that nuclear congression upon mating does depend on cytoplasmic microtubules attached to the half bridge, and thus is not affected by the deletion of *CNM67* (Brachat *et al.*, 1998). We tested whether this is also true for the *cnm67* partial deletions. As expected, these strains were proficient for uni- as well as for bilateral mating (our unpublished results). Therefore, the outer plaque structure alterations imposed by mutations in Cnm67p did not impair microtubule nucleation or binding at the half bridge.

Distance of Outer Plaque to Spindle Pole Body Core Is Adjusted by Cnm67p Coiled-Coil Region

The function of Cnm67p is affected less by mutations in the coil domain than it is by mutations in the N and C termini of the protein. This would suggest that only minor changes in SPB structure take place upon deletion of the *CNM67* coil domains. Electron microscopic analysis of SPBs of cells carrying a deletion of all three coil domains, *cnm67* Δ*coils*, has proven this to be true. The overall structure of the SPB remained intact, even with a much smaller gap between IL2 and the outer plaque (Figure 7, A–C). This suggests that the coils are mainly responsible for creating the space between these two layers. What could be the reasons for the low, but still significant nuclear migration defect of 17% observed in this mutant? First, the coiled-coil region might be required not for the localization of the outer plaque components, but for the assembly of Cnm67p into a support structure required for the formation of a fully functional outer plaque. This hypothesis is supported by our observation of disturbed outer plaque structures in the *cnm67* Δ*coils* mutant. Furthermore, an oligomerization of Cnm67p via the coil region has been suggested from two-hybrid interaction studies (Elliott *et al.*, 1999). Second, the decreased distance between IL2 and outer plaque might impose steric problems for the attachment of cytoplasmic microtubules to the outer plaque.

To further test the hypothesis of Cnm67p acting as a spacer element, we doubled its coiled-coil region and compared the distances between IL2 and OP of this *cnm67 2coils* mutant with the wild-type *CNM67* and *cnm67* Δ*coils* values (Figure 8). As anticipated, the distance between the outer plaque and the SPB core was extended in the *cnm67 2coils* mutant. For every addition or deletion of a coiled-coil region a variation in outer plaque to core distance of roughly 20 nm was observed (Figure 8B). Because the gap between IL2 and OP was almost absent in *cnm67* Δ*coils*-containing cells, we are confident that the coiled-coil region accounts for the gap in wild-type and in *cnm67 2coils* SPBs. With this assumption, based on the differences in OP-to-IL2 center distances, the length of the coiled-coil domain was calculated to be 20.3 nm. In a second approach, based on the gap differences, thereby taking the changes in outer plaque thickness into account, the calculated length of the coils was 19.7 nm. The data are in excellent agreement with existing SPB structural data (Bullitt *et al.*, 1997; O'Toole *et al.*, 1999). The average of 20 nm resulting from our calculations moreover shows a good correlation with the theoretical value of 25.65 nm predicted for an α3.6-helix with 1.5Å axial growth per residue, including all 169 amino acids in the heptad repeats required for coiled-coil formation (Brachat *et al.*, 1998; Figure 2A). It is possible that the shorter value of the measured coiled-coil length is caused by how the protein is assembled in the SPB, as it is not known to what extent the ends of the coiled-coil domains may be buried in IL2 or in the outer plaque. Because vertical striations connecting IL2, IL1, and OP are seen in some micrographs (O'Toole *et al.*, 1999), the SPB's IL1 layer might represent the center part of Cnm67p molecules aligned in parallel array.

In summary, we have shown that the essential regions of Cnm67p for its role in nuclear migration are located in the N- and C-terminal parts of this multidomain protein. The C terminus is required for its localization to the SPB. Cnm67p was demonstrated to be a phosphoprotein, and the phosphorylation sites map to the N-terminal domain. In this domain, several putative sites matching a consensus for Cdc28p phosphorylation can be found, and their role is currently under investigation. Structurally, our results demonstrate that Cnm67p has an important function in linking the outer plaque to the central plaque of the SPB. The distance of the outer plaque from IL2 is adjusted by the nonessential coiled-coil part of the protein. Several structural components of the *S. cerevisiae* SPB have been predicted to contain coiled-coil regions, namely, Spc42p of the central plaque (Donaldson and Kilmartin, 1996), Spc110p on the nuclear side of the SPB (Kilmartin *et al*., 1993), and Spc72 of the outer plaque (Knop and Schiebel, 1998; Souès and Adams, 1998). The spacer function of the SPB inner plaque has been assigned to Spc110p (Kilmartin *et al*., 1993). In this report we present several lines of evidence suggesting Cnm67p to be an analogous spacer on the cytoplasmic side of the SPB, determining the distance between the central and outer plaques.

ACKNOWLEDGMENTS

We thank Tom Giddings for advice on electron microscopy and C. Schaerer-Brodbeck for critical reading of the manuscript. This work has been supported by grants from the University of Basel to P.P. and by grants from the March of Dimes Birth Defects Foundation (1-FY00-55) and the National Institutes of Health (GM-51312) to M.W.

REFERENCES

Adams, I.R., and Kilmartin, J.V. (1999). Localization of core spindle pole body (SPB) components during SPB duplication in *Saccharomyces cerevisiae*. J. Cell Biol. *145*, 809–823.

Brachat, A., Kilmartin, J.V., Wach, A., and Philippsen, P. (1998). *Saccharomyces cerevisiae* cells with defective spindle pole body outer plaques accomplish nuclear migration via half-bridge-organized microtubules. Mol. Biol. Cell *9*, 977–991.

Bullitt, E., Rout, M.P., Kilmartin, J.V., and Akey, C.W. (1997). The yeast spindle pole body is assembled around a central crystal of Spc42p. Cell *89*, 1077–1086.

Byers, B. (1981). Cytology of the yeast life cycle. In: The Molecular Biology of the Yeast *Saccharomyces*. Life Cycle and Inheritance, ed. J.N. Strathern, E.W. Jones, and J.R. Broach, Cold Spring Harbor, NY: Cold Spring Harbor Laboratory, 59–96.

Byers, B., and Goetsch, L. (1975). Behavior of spindles and spindle plaques in the cell cycle and conjugation of *Saccharomyces cerevisiae*. J. Bacteriol. *124*, 511–523.

Carminati, J.L., and Stearns, T. (1997). Microtubules orient the mitotic spindle in yeast through dynein-dependent interactions with the cell cortex. J. Cell Biol. *138*, 629–641.

Chen, X.P., Yin, H., and Huffaker, T.C. (1998). The yeast spindle pole body component Spc72p interacts with Stu2p and is required for proper microtubule assembly. J. Cell Biol. *141*, 1169–1179.

Cormack, B.P., Bertram, G., Egerton, M., Gow, N.A., Falkow, S., and Brown, A.J. (1997). Yeast-enhanced green fluorescent protein (yEGFP), a reporter of gene expression in *Candida albicans*. Microbiology *143*, 303–311.

Cottingham, F.R., and Hoyt, M.A. (1997). Mitotic spindle positioning in *Saccharomyces cerevisiae* is accomplished by antagonistically acting microtubule motor proteins. J. Cell Biol. *138*, 1041–1053.

DeZwaan, T.M., Ellingson, E., Pellman, D., and Roof, D.M. (1997). Kinesin-related *KIP3* of *Saccharomyces cerevisiae* is required for a distinct step in nuclear migration. J. Cell Biol. *138*, 1023–1040.

Donaldson, A.D., and Kilmartin, J.V. (1996). Spc42: a phosphorylated component of the *S. cerevisiae* spindle pole body (SPB) with an essential function during SPB duplication. J. Cell Biol. *132*, 887–901.

Dower, W.J., Miller, J.F., and Ragsdale, C.W. (1988). High efficiency transformation of *Escherichia coli* by high voltage electroporation. Nucleic Acids Res. *16*, 6127–6145.

Elliott, S., Knop, M., Schlenstedt, G., and Schiebel, E. (1999). Spc29p is a component of the Spc110p subcomplex and is essential for spindle pole body duplication. Proc. Natl. Acad. Sci. USA *96*, 6205–6210.

Eshel, D., Urrestarazu, L.A., Vissers, S., Jauniaux, J.C., van Vliet-Reedijk, J.C., Planta, R.J., and Gibbons, I.R. (1993). Cytoplasmic dynein is required for normal nuclear segregation in yeast. Proc. Natl. Acad. Sci. USA *90*, 11172–11176.

Farkasovsky, M., and Küntzel, H. (1995). Yeast Num1p associates with the mother cell cortex during S/G2 phase and affects microtubular functions. J. Cell Biol. *131*, 1003–1014.

Francis, S.E., and Davis, T.N. (2000). The spindle pole body of *Saccharomyces cerevisiae*: architecture and assembly of the core components. In: The Centrosome in Cell Replication and Early Development, vol. 49, ed. R. E. Palazzo and G. P. Schatten, New York, NY: Academic Press, 105–132.

Friedman, D.B., Sundberg, H.A., Huang, E.Y., and Davis, T.N. (1996). The 100-kD spindle pole body component of *Saccharomyces cerevisiae* is a phosphoprotein that is modified in a cell-cycle dependent manner. J. Cell Biol. *132*, 903–914.

Gruneberg, U., Campbell, K., Simpson, C., Grindlay, J., and Schiebel, E. (2000). Nud1p links astral microtubule organization and the control of exit from mitosis. EMBO J. *19*, 6475–6488.

Hoepfner, D., Brachat, A., and Philippsen, P. (2000). Time-lapse video microscopy analysis reveals astral microtubule detachment in the yeast spindle pole mutant cnm67. Mol. Biol. Cell *11*, 1197–1211.

Horvath, A., and Riezman, H. (1994). Rapid protein extraction from yeast. Yeast *10*, 1305–1310.

Huffaker, T.C., Thomas, J.H., and Botstein, D. (1988). Diverse effects of beta-tubulin mutations on microtubule formation and function. J. Cell Biol. *106*, 1997–2010.

Huxley, C., Green, E.D., and Dunham, I. (1990). Rapid assessment of *S. cerevisiae* mating type by PCR. Trends Genet. *6*, 236.

Kellogg, D.R., Moritz, M., and Alberts, B.M. (1994). The centrosome and cellular organization. Annu. Rev. Biochem. *63*, 639–674.

Kilmartin, J.V. (1994). Genetic and biochemical approaches to spindle function and chromosome segregation in eucaryotic microorganisms. Curr. Opin. Cell Biol. *6*, 50–54.

Kilmartin, J.V., Dyos, S.L., Kershaw, D., and Finch, J.T. (1993). A spacer protein in the *Saccharomyces cerevisiae* spindle pole body whose transcript is cell cycle-regulated. J. Cell Biol. *123*, 1175–1184.

Knop, M., Pereira, G., Geissler, S., Grein, K., and Schiebel, E. (1997). The spindle pole body component Spc97p interacts with the gamma-tubulin of *Saccharomyces cerevisiae* and functions in microtubule organization and spindle pole body duplication. EMBO J. *16*, 1550–1564.

Knop, M., and Schiebel, E. (1997). Spc98p and Spc97p of the yeast gamma-tubulin complex mediate binding to the spindle pole body via their interaction with Spc110p. EMBO J. *16*, 6985–6995.

Knop, M., and Schiebel, E. (1998). Receptors determine the cellular localization of a gamma-tubulin complex and thereby the site of microtubule formation. EMBO J. *17*, 3952–3967.

Knop, M., Siegers, K., Pereira, G., Zachariae, W., Winsor, B., Nasmyth, K., and Schiebel, E. (1999). Epitope tagging of yeast genes using a PCR-based strategy: more tags and improved practical routines. Yeast *15*, 963–972.

Laemmli, U.K. (1970). Cleavage of structural proteins during the assembly of the head of bacteriophage T4. Nature *227*, 680–685.

Li, Y.Y., Yeh, E., Hays, T., and Bloom, K. (1993). Disruption of mitotic spindle orientation in a yeast dynein mutant. Proc. Natl. Acad. Sci. USA *90*, 10096–10100.

Lupas, A. (1996). Prediction and analysis of coiled-coil structures. Methods Enzymol. *266*, 513–525.

Miller, R.K., Matheos, D., and Rose, M.D. (1999). The cortical localization of the microtubule orientation protein Kar9p, is dependent upon actin and proteins required for polymerization. J. Cell Biol. *144*, 963–975.

Miller, R.K., and Rose, M.D. (1998). Kar9 is a novel cortical protein required for cytoplasmic microtubule orientation in yeast. J. Cell Biol. *140*, 377–390.

Mirzayan, C., Copeland, C.S., and Snyder, M. (1992). The *NUF1* gene encodes an essential coiled-coil related rotein that is a potential component of the yeast nucleoskeleton. J. Cell Biol. *116*, 1319–1332.

Moens, P.B., and Rapport, E. (1971). Spindles, spindle plaques, and meiosis in the yeast *Saccharomyces cerevisiae*. J. Cell Biol. *50*, 344–361.

Newman, J.R., Wolf, E., and Kim, P.S. (2000). From the cover: a computationally directed screen identifying interacting coiled coils from *Saccharomyces cerevisiae*. Proc. Natl. Acad. Sci. USA *97*, 13203–13208.

O'Toole, E.T., Winey, M., and McIntosh, J.R. (1999). High voltage electron tomography of spindle pole bodies and early mitotic spindles in the yeast *Saccharomyces cerevisiae*. Mol. Biol. Cell *10*, 2017–2031.

Palazzo, R.E., and Schatten, G.P. (ed) (2000). The Centrosome in Cell Replication and Early Development, New York, NY: Academic Press.

Palmer, R.E., Sullivan, D.S., Huffaker, T., and Koshland, D. (1992). Role of astral microtubules and actin in spindle orientation and migration in the budding yeast. *Saccharomyces cerevisiae*. J. Cell Biol. *119*, 583–593.

Pereira, G., Gruenenberg, U., Knop, M., and Schiebel, E. (1999). Interaction of the yeast gamma-tubulin complex-binding protein Spc72p with Kar1p is essential for microtubule function during karyogamy. EMBO J. *18*, 4180–4195.

Pereira, G., Knop, M., and Schiebel, E. (1998). Spc98p directs the yeast gamma-tubulin complex into the nucleus and is subject to cell cycle-dependent phosphorylation on the nuclear side of the spindle pole body. Mol. Biol. Cell *9*, 775–793.

Pereira, G., and Schiebel, E. (1997). Centrosome-microtubule nucleation. J. Cell Sci. *110*, 295–300.

Rout, M.P., and Kilmartin, J.V. (1990). Components of the yeast spindle and spindle pole body. J. Cell Biol. *111*, 1913–1927.

Sambrook, J., Fritsch, E.F., and Maniatis, T. (1989). Molecular Cloning: A Laboratory Manual, Cold Spring Harbor, NY: Cold Spring Harbor Laboratory.

Schaerer-Brodbeck, C., and Riezman, H. (2000). Interdependence of filamentous actin and microtubules for asymmetric cell division. Biol. Chem. *381*, 815–825.

Schiestl, R.H., and Gietz, R.D. (1989). High efficiency transformation of intact yeast cells using single stranded nucleic acids as a carrier. Curr. Genet. *16*, 339–346.

Shaw, S.L., Yeh, E., Maddox, P., Salmon, E.D., and Bloom, K. (1997). Astral microtubule dynamics in yeast: a microtubule-based searching mechanism for spindle orientation and nuclear migration into the bud. J. Cell Biol. *139*, 985–994.

Sikorski, R.S., and Hieter, P. (1989). A system of shuttle vectors and yeast host strains designed for efficient manipulation of DNA in *Saccharomyces cerevisiae*. Genetics *122*, 19–27.

Snyder, M. (1994). The spindle pole body of yeast. Chromosoma *103*, 369–380.

Souès, S., and Adams, I.R. (1998). *SPC72*: a spindle pole component required for spindle orientation in the yeast *Saccharomyces cerevisiae*. J. Cell Sci. *111*, 2809–2818.

Stirling, D.A., and Stark, M.J.R. (1996). The phosphorylation state of the 110 kDa component of the yeast spindle pole body shows cell cycle dependent regulation. Biochem. Biophys. Res. Commun. *222*, 236–242.

Sullivan, D.S., and Huffaker, T.C. (1992). Astral microtubules are not required for anaphase B in *Saccharomyces cerevisiae*. J. Cell Biol. *119*, 379–388.

Sundberg, H.A., and Davis, T.N. (1997). A mutational analysis identifies three functional regions of the spindle pole component Spc110p in *Saccharomyces cerevisiae*. Mol. Biol. Cell *8*, 2575–2590.

Wach, A., Brachat, A., Alberti-Segui, C., Rebischung, C., and Philippsen, P. (1997). Heterologous *HIS3* marker and GFP reporter modules for PCR-targeting in *Saccharomyces cerevisiae*. Yeast *13*, 1065–1075.

Wach, A., Brachat, A., Pöhlmann, R., and Philippsen, P. (1994). New heterologous modules for classical or PCR-based gene disruptions in *Saccharomyces cerevisiae*. Yeast *10*, 1793–1808.

Wigge, P.A., Jensen, O.N., Holmes, S., Souès, S., Mann, M., and Kilmartin, J.V. (1998). Analysis of the *Saccharomyces* spindle pole by matrix-assisted laser desorption/ionization (MALDI) mass spectrometry. J. Cell Biol. *141*, 967–977.

Winey, M., and Byers, B. (1993). Assembly and functions of the spindle pole body in budding yeast. Trends Genet. *9*, 300–304.

Winey, M., Mamay, C.L., O'Toole, E.T., Mastronarde, D.N., Giddings, T.H., Jr., McDonald, K.L., and McIntosh, J.R. (1995). Three-dimensional ultrastructural analysis of the *Saccharomyces cerevisiae* mitotic spindle. J. Cell Biol. *129*, 1601–1615.

Yanisch-Perron, C., Vieira, J., and Messing, J. (1985). Improved M13 phage cloning vectors and host strains: nucleotide sequences of the M13mp18 and pUC19 vectors. Gene *33*, 103–119.